JCTC Journal of Chemical Theory and Computation

pubs.acs.org/JCTC Article

Nonadiabatic Dynamics at Metal Surfaces: Fewest Switches Surface Hopping with Electronic Relaxation

Zuxin Jin* and Joseph E. Subotnik*

Cite This: *J. Chem. Theory Comput.* 2021, 17, 614–626 Read Online

ACCESS | Metrics & More | Article Recommendations

ABSTRACT: A new scheme is proposed for modeling molecular nonadiabatic dynamics near metal surfaces. The charge-transfer character of such dynamics is exploited to construct an efficient reduced representation for the electronic structure. In this representation, the fewest switches surface hopping (FSSH) approach can be naturally modified to include electronic relaxation (ER). The resulting FSSH-ER method is valid across a wide range of coupling strengths as supported by tests applied to the Anderson–Holstein model for electron transfer. Future work will combine this scheme with *ab initio* electronic structure calculations.

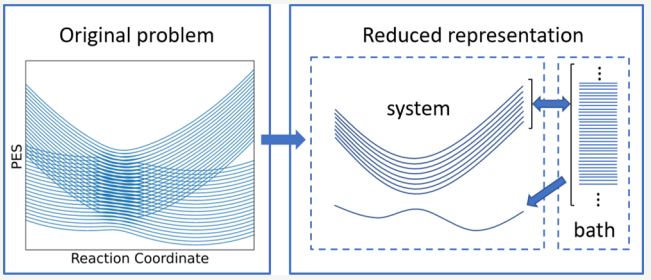

1. INTRODUCTION

Molecular nonadiabatic dynamics near metal surfaces has attracted widespread interest across many areas, including gas-phase scattering,[1−3] molecular junctions,[4−7] and dissociative chemisorption.[8−11] Because low-lying electron–hole pairs (EHPs) can be excited so easily in a metal, such dynamics can easily go beyond the Born–Oppenheimer approximation, as indicated by various phenomena like chemicurrents,[12,13] unusual vibrational relaxation,[14−17] and inelastic scattering.[18−20] Therefore, to fully understand these processes, a robust approach to nonadiabatic dynamics would be extremely useful. Nevertheless, in spite of the enormous progress made to date,[21−44] modeling such dynamics remains a very difficult task and poses tough problems for both electronic structure calculations and dynamics simulations.

In terms of the electronic structure, the heterogeneous nature of a molecule–metal interface raises a basic question: what is the appropriate representation for describing a typical molecule–metal system? In particular, two sub-questions must be addressed:

First, should we adopt a simple picture of independent (or mean-field) electrons or a more complex picture of interacting electrons? The former is far more efficient than the latter and is known to be adequate in many systems. However, it is dubious whether an independent electron picture is sufficient for the majority of the reactions. After all, for molecules alone (i.e., without a metal), a high-level electronic structure method is usually necessary if we are to model bond making and bond breaking:[45−47] Why should the presence of a metal make the problem that much simpler?

Second, note that while the entire system possesses a large number of electronic degrees of freedom (DoFs), the number of distinct molecular electronic states is always much smaller. Thus, if one is only interested in the molecular dynamics, one can ask: is it necessary to work with the entire system's adiabatic states (or one-electron eigenstates), or can we safely seek a reduced representation? A reduced picture would be far more computationally attractive/feasible. However, what would be a good enough reduced picture? Would a simple molecular diabatic representation suffice, or must we seek a more accurate alternative?

Next, let us turn to nuclear dynamics. In a fully quantum picture, when a nuclear wave packet passes through a crossing with nonvanishing coupling, the wave packet splits into individual wave packets each associated with individual electronic potential energy surfaces (PESs). This picture lies at the heart of nonadiabatic dynamics, and it remains valid at both high and low temperatures. However, because of the formidable cost of simulating quantum nuclei and the fact that kT in many scenarios is larger than the characteristic energy of low-frequency nuclear motion, semi-classical approaches have become popular today. Quite often, a nuclear wave packet and its splitting near a crossing is modeled by an ensemble of classical trajectories and their branching. Nevertheless, in order to achieve a quantitative description, many approximations will be necessary, some of which are uncontrolled and will need to

Received: September 24, 2020
Published: January 29, 2021

https://dx.doi.org/10.1021/acs.jctc.0c00997
J. Chem. Theory Comput. 2021, 17, 614–626

be analyzed against accurate benchmark studies. For the present paper, we will assume that a classical simulation of nuclei is sufficient, and we will focus on all of the other problems that arise as far as nonadiabatic effects.

When simulating nuclear dynamics at a metal surface, it cannot be emphasized enough both (i) that capturing the dynamics accurately requires modeling many electronic states to represent the continuum and (ii) that modeling so many electronic states can be a computational quagmire. This situation can and should be contrasted with the case of nonadiabatic dynamics involving only a handful of discrete electronic states, for example, a gas-phase photo-excited molecule, where there are many tools for solving for an electronic structure and studying nonadiabatic dynamics. For instance, for a molecule in the gas phase, accurate excited PESs can often be achieved by time-dependent density functional theory (DFT) or multiconfiguration self-consistent field methods; if necessary, adiabatic-to-diabatic transformations can be performed to generate a diabatic picture; and finally, a variety of (nearly) exact dynamical schemes have been proposed, including the Miller–Meyer–Stock–Thoss approach,[48,49] multiconfiguration time-dependent Hartree,[50−54] multiple spawning,[55] hierarchical quantum master equation,[56−60] quantum Monte-Carlo,[61−64] linearized density matrix dynamics,[65,66] and so forth. While many of these methods do in principle allow an arbitrary number of electronic DoFs and some of them have been applied to systems with a fermionic bath,[61−64,67−69] it remains a difficult task to treat a realistic *ab initio* Hamiltonian with a continuum of electronic states in the presence of a large number of anharmonic vibrational modes. For the present problem, the number of energetically relevant excited states is prohibitively large because of the possibility of exciting low-lying EHPs.

Beyond the requirement of handling a large number of electronic states, another difficulty when modeling nuclear-electronic dynamics at a metal surface is the need for accurate dynamics across a wide range of parameters. For a molecule near a metal surface, there are at least three characteristic energy scales: the temperature kT, the hybridization function Γ, and the characteristic energy scale of nuclear motion $\hbar\omega$. Assuming $kT \gg \hbar\omega$, so that nuclear motion can be viewed classical, there are well-established methods that apply to different regions of Γ, as illustrated by Figure 1.[27] Specifically,

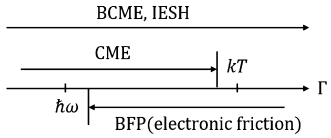

Figure 1. Coverage of the CME and the broadened Fokker–Planck method with respect to the hybridization function, assuming $kT \gg \hbar\omega$. This figure is adapted from Figure 1 of ref 27.

for $\Gamma < kT$, one arrives at a classical master equation (CME), in which the effect of the metal can be captured by stochastic hops between molecular diabatic surfaces;[31,70,71] for $\Gamma > \hbar\omega$, it has been shown that nonadiabatic effects on nuclear dynamics can be well incorporated into the electronic friction tensor,[29,30,72−84] leading to a Langevin dynamics on a potential of mean force (PMF).[81]

However, nuclear dynamics in the above two regions are not directly compatible with each other (though, see our description of the BCME in Section 1.1 below). Moreover, for realistic systems, both scenarios are possible, and, more often than not, a system may sample both regions in a single experiment. Thus, a method that works in both limits is needed.

1.1. Existing Semi-classical Approaches to Nonadiabatic Dynamics at Metal Surfaces. Before presenting a new algorithm for such dynamics (below in Section 2), a few more cautionary words are needed to help refine the scope of the problem. To the best of our knowledge, there are, today, two principal algorithms for simulating nonadiabatic dynamics near a metal surface semi-classically that should be valid across a wide range of parameter regimes. The first method is the independent electron surface hopping (IESH),[24,25,85] which is a variant of the famous fewest-switches surface hopping (FSSH).[86] According to IESH, one allows individual electrons to hop between orbitals, eventually gathering statistics. As such, a single Slater determinant can capture a vast number of excited states. In practice, IESH has been applied to the NO–Au scattering experiment[26] and often gives qualitatively good results. Nevertheless, by definition, the independent electron picture cannot be extended to systems whose electronic structures are correlated beyond a mean-field approximation.

A second approach to this same problem is the broadened CME (BCME),[27,87] which was recently developed by our research group and compared with IESH.[88] As mentioned above, a CME is a perturbative approach to nonadiabatic dynamics that is equivalent to stochastic motion along raw diabatic PESs (e.g., PESs corresponding to charge or noncharged states)—this approach is valid only for very small molecular-metal coupling ($\Gamma < kT$). In order to go beyond this limitation, the BCME extrapolates the motion from raw diabatic PESs to "broadened" diabatic PESs so that, altogether, nuclear motion recovers the proper PMF (for $\Gamma < kT$ or $\Gamma > kT$). A schematic diagram of the broadened diabats is shown in Figure 2 for the noninteracting Anderson–Holstein model, for which the BCME has been shown to yield accurate and efficient results.[88,89] Recently, the BCME has also been applied to model electrochemical problems.[90] Now, at bottom, because the BCME is formulated in a modified molecular diabatic picture, such a construction has natural

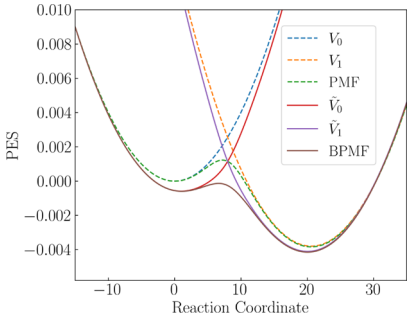

Figure 2. Schematic diagram of the relevant PESs for the noninteracting Anderson–Holstein model. The dashed lines correspond to the raw (e.g., perturbative) impurity diabats and PMF as relevant in the limit $\Gamma < kT$ (and as used by a CME); and the solid lines are their broadened counterparts as applicable when $\Gamma < kT$ or $\Gamma > kT$ (and as used by the BCME). By performing CME-like dynamics on broadened diabats, the BCME is able to work in the $\Gamma > kT$ regime and recover the correctly broadened barrier between the well on the left and the well on the right; note that the correctly broadened PMF can be much lower than the unbroadened PMF at the crossing point. More details about the BCME can be found in refs 27,28,88,90.

https://dx.doi.org/10.1021/acs.jctc.0c00997
J. Chem. Theory Comput. 2021, 17, 614−626

upsides and downsides. The upside is that, by construction, the BCME is very inexpensive because it does not need to treat a large number of electronic states explicitly (as opposed to IESH where all one-electron eigenstates are explicitly involved). The downside is that the method is not easily applied to realistic systems where one would like to perform *ab initio* electronic structure calculations rather than estimate broadened diabats and a hybridization function that is forced to obey the wide-band approximation (WBA).

Ultimately, the holy grail for nonadiabatic molecular dynamics on a surface is a computationally feasible algorithm that works in the weak and strong coupling limits, can be easily applied to either model or ab initio electronic Hamiltonians, and which can treat electron−electron interactions correctly.

1.2. FSSH with ER (FSSH-ER). With this background in mind, we will now present a new algorithm which will satisfy many of the desired properties, though with a cost more than the BCME algorithm.[91] The method should be compatible with *ab initio* electronic structure calculations and be able to treat electron correlation correctly; future publications will hopefully confirm these two assertions.

Working in the context of the (noninteracting) Anderson−Holstein model, our specific approach will be as follows: First, we will start with a set of one-electron eigenstates (similar to IESH) but then (unlike IESH), we will invoke a Schmidt decomposition to find pairs of Schmidt orbitals (one localized on the molecule and one localized on the metal). This pair of orbitals is analogous to the two molecular diabatic states that one would predict with a theory like the BCME. Second, we will use these Schmidt orbitals to construct an appropriate subspace of many-electron Slater determinants from which we can build a configuration interaction Hamiltonian. Third and finally, we will apply a modified version of the FSSH to our system. Below, we will show that this nonadiabatic dynamics protocol is able to recapitulate Marcus's electrochemical theory (in the nonadiabatic limit) as well as transition state theory (TST) (in the adiabatic limit), which gives us hope that this new framework may be quite powerful going forward. The electronic structure and dynamics algorithms above should have natural extensions to *ab initio* calculations beyond the Anderson−Holstein model.

Regarding the outline of the article, in Section 2, we present the theory described above, including the necessary choice of electronic states and the proposed protocol for running nuclear-electronic dynamics. In Section 3, we present results for the Anderson−Holstein model, which describes electron transfer at a metal surface in an idealized fashion and is the basis of Marcus theory at a metal surface. In Section 4, we discuss our results, emphasizing a few nuances of the present algorithm (that may have gone unappreciated) and highlighting future numerical tests of the current protocol. We conclude in Section 5.

2. METHOD

In this work, we assume that the electronic Hamiltonian for the system of a molecule near a metal surface can be represented by the Anderson−Holstein model

$$H_e(\boldsymbol{R}) = U_0(\boldsymbol{R}) + \epsilon_d(\boldsymbol{R}) d^\dagger d + \sum_k \epsilon_k c_k^\dagger c_k + \sum_k (V_k(\boldsymbol{R}) d^\dagger c_k + V_k^*(\boldsymbol{R}) c_k^\dagger d) \quad (1)$$

here, $\boldsymbol{R}$ represents the nuclear coordinate; d is the fermionic operator for the molecular orbital whose on-site energy is ϵ_d; $U_0(\boldsymbol{R})$ and $U_1(\boldsymbol{R}) \equiv U_0(\boldsymbol{R}) + \epsilon_d(\boldsymbol{R})$ are the two molecular diabatic PESs; c_k is the operator for the metal state k whose energy is ϵ_k; and V_k is the hopping amplitude between the molecular orbital and the metal state k.

The hybridization function Γ is defined to be

$$\Gamma(\epsilon, \boldsymbol{R}) = 2\pi \sum_k |V_k(\boldsymbol{R})|^2 \delta(\epsilon - \epsilon_k) \quad (2)$$

which, roughly speaking, represents the rate of electronic relaxation (ER) of the impurity orbital. Of course, for realistic systems, Γ should depend on both ϵ and $\boldsymbol{R}$, so its relation to the rate is not obvious in general. In many scenarios, however, one can adopt the WBA, where Γ is assumed to be independent of ϵ; in such a case, if $\boldsymbol{R}$ is held fixed (or in the hypothetical case that Γ was also independent of $\boldsymbol{R}$), Γ becomes exactly the rate of ER. Note that the method presented in this paper does not, in principle, rely on any of these assumptions for Γ; for simplicity, however, the example given in Section 3 does assume that Γ is a constant so that the discussion on characteristic energy scales is less ambiguous.

Equation 1 can represent a molecule−metal system only when $\{\epsilon_k\}$ forms a quasi-continuum such that the energy spacing of ϵ_k is smaller than any relevant characteristic energy scale (which includes Γ, of course). This noninteracting Hamiltonian can be directly diagonalized

$$H_e(\boldsymbol{R}) = U_0(\boldsymbol{R}) + \sum_p \lambda_p(\boldsymbol{R}) b_p^\dagger b_p \quad (3)$$

and its ground state is a Slater determinant

$$|\Psi_0\rangle = |ij...\rangle \quad (4)$$

where $ij...$ are occupied orbitals.

For a noninteracting Hamiltonian like eq 1, the above ground state is exact. For realistic systems where there are electron−electron interactions, a ground state of the form of a Slater determinant can usually be constructed by assuming a mean-field ansatz—which may or may not be valid. We will assume that eq 4 is valid throughout this work, but see Section 4.2 and ref 92 for our initial steps toward treating electron−electron interactions.

In order to model nonadiabatic dynamics, electronic excited states must be considered. While such electronically excited states can be delineated by counting all of the possible configuration states ($|\Psi_i^a\rangle$, $|\Psi_{ij}^{ab}\rangle$,...), the total number of such states is enormous and forbids a direct application of conventional mixed quantum-classical methods like the FSSH. To address this problem, IESH[24] was introduced as a variant of the FSSH. By allowing electrons to hop individually between orbitals (instead of working with a many electron basis), IESH effectively samples a vast number of possible configuration states. Nevertheless, this assumption also makes IESH difficult to extend to systems where electron−electron interactions and correlations become significant. Below, we will propose another variant of the FSSH. In particular, we will use a reduced many electron description that focuses on charge-transfer nonadiabatic effects.

2.1. Construction of a Reduced Representation. *2.1.1. Orbital Rotation.* An important fact about Slater determinants is that they are invariant under a unitary transformation of their orbitals. Given the definition of $|\Psi_0\rangle$

https://dx.doi.org/10.1021/acs.jctc.0c00997
J. Chem. Theory Comput. 2021, 17, 614−626

in eq 4, let U be a unitary matrix, and $|\tilde{j}\rangle = \sum_i^{\mathrm{occ}} |i\rangle U_{ij}$ be a set of new orthonormal orbitals. Then, $|\tilde{\Psi}_0\rangle \equiv |\tilde{i}\tilde{j}...\rangle = \det(U)|\Psi_0\rangle$ differs from the canonical ground state (eq 4) by merely a phase. In other words, $|\tilde{\Psi}_0\rangle$ and $|\Psi_0\rangle$ are the same many body state. This degree of freedom has previously been exploited for various purposes, including the generation of localized molecular orbitals[93−95] and construction of an active space in density matrix embedding theory (DMET).[96,97]

If one wishes to use a basis of configurations to extract to excited states, one must expect that the optimal and most efficient set of orbitals should capture the physical character (e.g., charge character) of the excited states (as opposed to the canonical orbitals). For a molecule near a metal surface, some of the most interesting nonadiabatic effects originate from the possibility of charge transfer between the molecule and the metal. This predicament indicates that, for our purposes, one would like to find a new set of orbitals which separate the molecule and metal components (even if there is strong mixing via covalent bonds).

Here, we suggest rotating the canonical orbitals according to the following procedure. First, we project the localized molecular orbital onto the occupied and virtual spaces, respectively

$$|d_{\mathrm{o}}\rangle \equiv \frac{1}{\sqrt{\langle n\rangle}} \sum_i^{\mathrm{occ}} |i\rangle\langle i|d\rangle \tag{5a}$$

$$|d_{\mathrm{v}}\rangle \equiv \frac{1}{\sqrt{1-\langle n\rangle}} \sum_a^{\mathrm{vir}} |a\rangle\langle a|d\rangle \tag{5b}$$

where $\langle n\rangle = \sum_i^{\mathrm{occ}} |\langle i|d\rangle|^2$ is the impurity population of the ground state. Next, we orthonormalize the occupied and virtual spaces, respectively, while keeping $|d_{\mathrm{o}}\rangle$ and $|d_{\mathrm{v}}\rangle$ unchanged (this can be achieved by a QR decomposition with $|d_{\mathrm{o}}\rangle$ or $|d_{\mathrm{v}}\rangle$ being the first orbital). This leads to an occupied subspace space $\{|d_{\mathrm{o}}\rangle,\{|\tilde{i}\rangle\}\}$ and a virtual subspace $\{|d_{\mathrm{v}}\rangle,\{|\tilde{a}\rangle\}\}$. We refer to $\{|\tilde{i}\rangle\}$ as the occupied bath space and $\{|\tilde{a}\rangle\}$ the virtual bath space. Note that the bath orbitals $|\tilde{i}\rangle$ and $|\tilde{a}\rangle$ are not uniquely determined at this stage because a unitary transformation within each bath space is still allowed. To specify the bath orbitals, we demand that the Hamiltonian in the bath subspace be diagonal. This constraint can be achieved as follows. Let $\{\tilde{i}'\}$ and $\{\tilde{a}'\}$ denote the "raw" bath orbitals that result from the orthonormalization. Construct the subspace Hamiltonians $\tilde{H}^{\mathrm{occ}}_{ij} \equiv \langle\tilde{i}'|H|\tilde{j}'\rangle$ and $\tilde{H}^{\mathrm{vir}}_{ab} \equiv \langle\tilde{a}'|H|\tilde{b}'\rangle$. By diagonalizing $\tilde{H}^{\mathrm{occ}}$ and $\tilde{H}^{\mathrm{vir}}$

$$\tilde{H}^{\mathrm{occ}} = \tilde{V}^{\mathrm{occ}}\tilde{\Lambda}^{\mathrm{occ}}(\tilde{V}^{\mathrm{occ}})^{\dagger} \tag{6a}$$

$$\tilde{H}^{\mathrm{vir}} = \tilde{V}^{\mathrm{vir}}\tilde{\Lambda}^{\mathrm{vir}}(\tilde{V}^{\mathrm{vir}})^{\dagger} \tag{6b}$$

it is readily seen that the following rotations

$$|\tilde{i}\rangle = \sum_j |\tilde{j}'\rangle\tilde{V}^{\mathrm{occ}}_{ji} \tag{7a}$$

$$|\tilde{a}\rangle = \sum_b |\tilde{b}'\rangle\tilde{V}^{\mathrm{vir}}_{ba} \tag{7b}$$

generate bath orbitals that fulfill our requirements, say

$$\langle\tilde{i}|H|\tilde{j}\rangle = \Lambda_{ii}\delta_{ij} \tag{8a}$$

$$\langle\tilde{a}|H|\tilde{b}\rangle = \Lambda_{aa}\delta_{ab} \tag{8b}$$

This procedure uniquely defines the bath orbitals (up to some phase) and finalizes the orbital rotation.

To summarize, we suggest an orbital rotation in each of the occupied and virtual subspaces in such a way that the Hamiltonian in the new basis now appears as follows

$$H = \begin{array}{c} \begin{array}{cccc} d_o & \tilde{i} & & d_v \quad \tilde{a} \end{array} \\ \begin{bmatrix} * & * & \cdots & 0 \\ * & & & \\ \vdots & & & \\ 0 & & & \\ & & * & * \\ & & * & \\ & & \vdots & \end{bmatrix} \end{array} \tag{9}$$

Because the rotation does not mix occupied and virtual orbitals, the Hamiltonian in the new basis retains a block-diagonal structure where the two blocks correspond to the occupied and virtual subspace, respectively. Each block, instead of being diagonal (as is the case with canonical orbital basis), now appears to be an impurity Hamiltonian. This orbital rotation can be understood as a Schmidt decomposition and is similar to the DMET active space construction.[96,97] In the context of DMET, $|d_{\mathrm{o}}\rangle$ is the Schmidt orbital related to $|d\rangle$. After the rotation, only $|d_{\mathrm{o}}\rangle$ and $|d_{\mathrm{v}}\rangle$ can possibly have nonzero impurity components; all the bath orbitals lie entirely in the metal.

2.1.2. Configuration Basis. With the rotated orbitals defined above, configurations can be categorized according to whether they involve molecular excitations or not. For example, $|\Psi^{\tilde{a}}_{d_{\mathrm{o}}}\rangle$ represents a charge-transfer excitation from the molecule to the metal, while $|\Psi^{\tilde{a}}_{\tilde{i}}\rangle$ is an EHP excitation located completely in the metal. For the purpose of simulating molecular nonadiabatic dynamics near a metal surface, configurations that involve molecular excitations are more important than pure-bath excitations; this idea lies at the heart of our reduced representation.

We now make our first major approximation. We assume that only configuration interaction singles are needed for an accurate enough electronic structure; double excitations and beyond are completely ignored. This approximation can be understood as assuming "fast bath equilibration", that is, all configurations which involve more than two bath orbitals relax immediately. For the pair of Schmidt orbitals, note that $\sqrt{\langle n\rangle}|d_{\mathrm{o}}\rangle + \sqrt{1-\langle n\rangle}|d_{\mathrm{v}}\rangle = |d\rangle$ and its complement $|d^*\rangle \equiv -\sqrt{1-\langle n\rangle}|d_{\mathrm{o}}\rangle + \sqrt{\langle n\rangle}|d_{\mathrm{v}}\rangle$ is completely localized to the metal ($\langle d|d^*\rangle = 0$), so $|d_{\mathrm{o}}\rangle$ and $|d_{\mathrm{v}}\rangle$ together contribute to one bath orbital. Specifically, if ϵ_{d} is far below the Fermi level, then $|d_{\mathrm{o}}\rangle \approx |d\rangle$ and $|d_{\mathrm{v}}\rangle$ is almost completely localized to the metal; if ϵ_{d} is far above the Fermi level, then $|d_{\mathrm{v}}\rangle \approx |d\rangle$ and $|d_{\mathrm{o}}\rangle$ is almost completely localized to the metal; and if ϵ_{d} is around the Fermi level, then both $|d_{\mathrm{o}}\rangle$ and $|d_{\mathrm{v}}\rangle$ are partially localized to the metal.

The single excitation states contain the following four categories

https://dx.doi.org/10.1021/acs.jctc.0c00997
J. Chem. Theory Comput. 2021, 17, 614−626

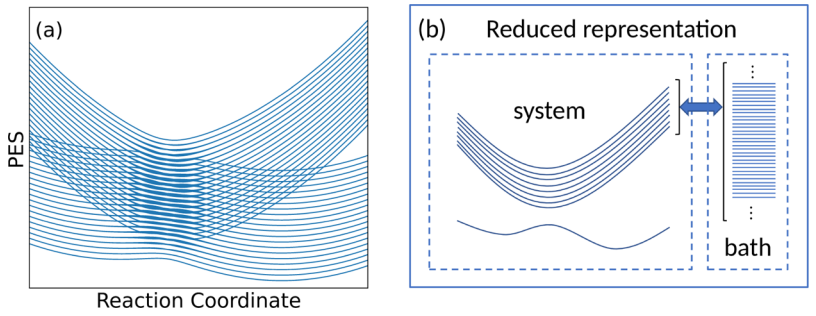

Figure 3. Schematic diagram of the reduced representation. (a) Original PESs for a molecule−metal system. (b) Reduced representation for (a). Each excited state in the reduced system is coupled to the reduced bath.

$$\{|\Psi_{d_o}^{d_v}\rangle,\ \{|\Psi_{d_o}^{\tilde{a}}\rangle\},\ \{|\Psi_{\tilde{i}}^{d_v}\rangle\},\ \{|\Psi_{\tilde{i}}^{\tilde{a}}\rangle\}\} \tag{10}$$

Among these four categories, the first three are relevant to the excitations on the molecule, while the last one merely contains bath excitations. We therefore define

$$\Omega_S \equiv \{|\Psi_0\rangle,\ |\Psi_{d_o}^{d_v}\rangle,\ \{|\Psi_{d_o}^{\tilde{a}}\rangle\},\ \{|\Psi_{\tilde{i}}^{d_v}\rangle\}\} \tag{11}$$

to be the "reduced system space" of dynamical interest, and

$$\Omega_B \equiv \{|\Psi_{\tilde{i}}^{\tilde{a}}\rangle\} \tag{12}$$

to be the corresponding "reduced bath space".

We emphasize that Ω_S and Ω_B are not the physical impurity system or bath; states in Ω_S have nonzero amplitude on the metal and states in Ω_B have nonzero amplitude on the molecule. Here, Ω_S contains a subset of the possible states of the entire system during a dynamical process. This subset is selected with a special focus on the molecular charge character, which we believe to be the most important ingredient for the molecular charge-transfer nondiabatic dynamics. In particular, $\{|\Psi_{d_o}^{\tilde{a}}\rangle\}$ should capture potential one-electron transfer from the molecule to the metal, and $\{|\Psi_{\tilde{i}}^{d_v}\rangle\}$ should capture potential one-electron transfer from the metal to the molecule.

Finally, to finish the construction of the reduced representation, let us now focus on Ω_S and Ω_B in turn:

- The reduced system (adiabatic) states, denoted $|\Psi_J\rangle$, are defined as those which diagonalize the system Hamiltonian in Ω_S

$$|\Psi_J\rangle = c_0^{(J)}|\Psi_{d_o}^{d_v}\rangle + \sum_{\tilde{i}} c_{\tilde{i}}^{(J)}|\Psi_{\tilde{i}}^{d_v}\rangle + \sum_{\tilde{a}} c_{\tilde{a}}^{(J)}|\Psi_{d_o}^{\tilde{a}}\rangle \qquad (J > 0) \tag{13a}$$

$$\langle\Psi_J|H|\Psi_{J'}\rangle = E_J\delta_{JJ'} \tag{13b}$$

Note that the original ground state $|\Psi_0\rangle$ does not couple to the single excitations, so it remains the ground adiabatic state in our reduced system. Our reduced system has really just introduced a new set of excited adiabatic states.

- $|\Psi_{\tilde{i}}^{\tilde{a}}\rangle$ are defined to be the reduced bath states. By enforcing eqs 8a and 8b, these bath states are naturally the eigenstates of H in Ω_B

$$\langle\Psi_{\tilde{i}}^{\tilde{a}}|H|\Psi_{\tilde{j}}^{\tilde{b}}\rangle = \delta_{\tilde{i}\tilde{j}}\delta_{\tilde{a}\tilde{b}}(E_0 - \lambda_{\tilde{i}} + \lambda_{\tilde{a}}) \tag{14}$$

The entire reduced representation contains the reduced system states and the reduced bath states as pictured schematically in Figure 3.

The reduced representation defined above forms a new impurity model. For the J-th system adiabatic state, we can define the hybridization function in a manner similar to eq 2

$$\widetilde{\Gamma}_J(E) = 2\pi\sum_{\tilde{i}\tilde{a}} |\langle\Psi_J|H|\Psi_{\tilde{i}}^{\tilde{a}}\rangle|^2\,\delta(E - E_{\tilde{i}}^{\tilde{a}}) \qquad (J > 0) \tag{15}$$

2.2. FSSH with ER (FSSH-ER). *2.2.1. Electronic Dynamics.* Within conventional FSSH, all electronic states are evolved according to the full electronic Hamiltonian. Armed with a finite number of adiabatic states and bath states defined above, we will now present a new variant of the FSSH method which includes explicit ER to account for the presence of a truly infinite metal. To do so, for a set of system states (defined in eqs 13a and 13b and which are explicitly coupled to a bath), the system's electronic dynamics follow a Lindblad equation in the Markovian limit

$$\frac{\mathrm{d}\rho_S t}{\mathrm{d}t} = -\frac{i}{\hbar}[H_S, \rho_S] + \mathcal{L}(\rho_S) \tag{16a}$$

$$\mathcal{L}(\rho) \equiv \sum_J \gamma_J\left(L_J\rho L_J^\dagger - \frac{1}{2}\{L_J^\dagger L_J, \rho\}\right) \tag{16b}$$

here, ρ_S is the system density matrix, H_S is the Hamiltonian in Ω_S subspace, γ_J is a non-negative number related to the rate of relaxation, L_J is the Lindblad jump operator, and $\{\cdot,\cdot\}$ is the anticommutator.

We now make our second major approximation. We assume that all of the system excited states $\{|\Psi_J\rangle\}$ relax to the ground state at a rate given by the new hybridization function defined in eq 15 as evaluated at the relevant adiabatic energy, namely

$$\gamma_J = \widetilde{\Gamma}_J(E_J) \tag{17}$$

This approximation is consistent with the premise of "fast bath equilibration", only now stronger; we assume that, once the system states relax to the bath states, those bath states immediately return to the ground state.

As for the Lindblad jump operators, we choose them to be of the form

$$(L_J)_{KL} = \delta_{K0}\delta_{LJ}\sqrt{1 - f_J} + \delta_{KJ}\delta_{L0}\sqrt{f_J} \qquad (J > 0) \tag{18}$$

where

$$f_J \equiv \frac{1}{e^{\beta(E_J - E_0)} + 1} \tag{19}$$

It is easy to verify that the diagonal elements are

https://dx.doi.org/10.1021/acs.jctc.0c00997
J. Chem. Theory Comput. 2021, 17, 614−626

$$(\mathcal{L}(\rho))_{00} = \sum_{J>0} \widetilde{\Gamma}_J(\rho_{JJ}(1-f_J) - \rho_{00}f_J) \tag{20a}$$

$$(\mathcal{L}(\rho))_{KK} = \widetilde{\Gamma}_K(\rho_{00}f_K - \rho_{KK}(1-f_K)) \qquad (K>0) \tag{20b}$$

which ensure the correct ER. The off-diagonal elements are

$$(\mathcal{L}(\rho))_{0K} = \Gamma_K\sqrt{f_K(1-f_K)}\rho_{K0} - \frac{1}{2}\left(\Gamma_K(1-f_K) + \sum_{J>0}\Gamma_J f_J\right)\rho_{0K} \qquad (K>0) \tag{21}$$

$$(\mathcal{L}(\rho))_{JK} = -\frac{1}{2}(\Gamma_J(1-f_J) + \Gamma_K(1-f_K))\rho_{JK} \quad (J,K>0,\ J\neq K) \tag{22}$$

$$(\mathcal{L}(\rho))_{K0} = (\mathcal{L}(\rho))^*_{0K} \tag{23}$$

In the zero-temperature limit ($f_J = 0$ for any $J > 0$), eqs 21 and 22 reduce to

$$(\mathcal{L}(\rho))_{0K} = -\frac{1}{2}\Gamma_K\rho_{0K} \qquad (K>0) \tag{24}$$

$$(\mathcal{L}(\rho))_{JK} = -\frac{1}{2}(\Gamma_J + \Gamma_K)\rho_{JK} \qquad (J,K>0,\ J\neq K) \tag{25}$$

2.2.2. Surface Switching. According to Tully's FSSH protocol, one switches between surfaces at a rate which guarantees that the proportion of nuclear trajectories on each PES agrees with the instantaneous density matrix. To understand how this is achieved, note that, according to the time-dependent Schrödinger equation

$$\frac{d\rho_{JJ}}{dt} = -\sum_{K\neq J} 2\mathcal{R}e\{T_{JK}\rho_{KJ}\} \equiv -\sum_{K\neq J} g_{KJ} \tag{26}$$

where $T_{JK} \equiv \langle J|(\partial/\partial t)|K\rangle$ is the time-derivative coupling. The FSSH algorithm then requires that, at each time step, for a trajectory moving along state J, one switches to state K in FSSH with probability

$$P_{K\leftarrow J} = \Delta t\frac{g_{KJ}}{\rho_{JJ}}\Theta(g_{KJ}) \tag{27}$$

where Θ is the Heaviside step function. If the fraction of nuclear trajectories agrees with the electronic density matrix at one time step, then, with the hopping probability above, the change in the population for state J is

$$\begin{aligned}\Delta F_J &= \sum_{K\neq J}(-P_{K\leftarrow J}\rho_{JJ} + P_{J\leftarrow K}\rho_{KK}) \\ &= \Delta t\sum_{K\neq J}(-g_{KJ}\Theta(g_{KJ}) + g_{JK}\Theta(g_{JK})) \\ &= -\Delta t\sum_{K\neq J} g_{KJ} = \Delta\rho_{JJ}\end{aligned} \tag{28}$$

Here, we have used both eq 26 and the fact that g is antisymmetric, $g_{JK} = -g_{KJ}$. As such, after a time step Δt, Tully's algorithm should keep the fraction of nuclear trajectories on each state in agreement with the electronic density matrix.[98]

With this consistency in mind because of the extra relaxation term for the electronic dynamics in eqs 16a and 16b, we will need to alter the surface switching algorithm accordingly. To be specific, we need to express eqs 20a and 20b as a sum of antisymmetric terms (just as in eq 26). A convenient choice is

$$\zeta_{KJ} \equiv \delta_{K0}\widetilde{\Gamma}_J(\rho_{JJ}(1-f_J) - \rho_{00}f_J) - \delta_{J0}\widetilde{\Gamma}_K(\rho_{KK}(1-f_K) - \rho_{00}f_K) \tag{29}$$

$$\frac{d\rho_{JJ}}{dt} = -\sum_{K\neq J}(g_{KJ} + \zeta_{KJ}) \tag{30}$$

Consequently, we also modify eq 27 as follows

$$P_{K\leftarrow J} = \Delta t\frac{g_{KJ} + \zeta_{KJ}}{\rho_{JJ}}\Theta(g_{KJ} + \zeta_{KJ}) \tag{31}$$

2.2.3. Momentum Rescaling and Velocity Reversal. According to FSSH-ER, as one can see from eq 30, a hop can be initiated by either the derivative coupling (the g term) or ER (the ζ term). This state of affairs is to be contrasted with standard FSSH, where there is no ER, which leads to another question vis-a-vis FSSH-ER. Namely, within standard FSSH, when a hop is successful, the momentum of the nuclear trajectory is rescaled to conserve the energy. This procedure is natural for a closed system but is not appropriate for the open system we defined in Section 2.1: after all, energy released by ER is dissipated into a bath rather than the molecule, and the reduced system should not conserve energy. Therefore, consistent momentum rescaling at every hop is not appropriate, and a new protocol is required for FSSH-ER.

To address this issue, we suggest that if a successful hop is initiated by the derivative coupling, the momentum is rescaled as usual and if a hop is initiated by the ER, the momentum is not rescaled. Specifically, consider a successful hop from state J to state K. If $g_{KJ} > 0$ and $\zeta_{KJ} < 0$, momentum is rescaled as usual; if $g_{KJ} < 0$ and $\zeta_{KJ} > 0$, momentum is not rescaled; and if $g_{KJ} > 0$ and $\zeta_{KJ} > 0$, an additional random number r with $0 < r < 1$ is generated and the momentum is rescaled if $r < g_{KJ}/(g_{KJ} + \zeta_{KJ})$.

Now, in practice, another important component for FSSH is the velocity reversal as suggested by Japser and Truhlar,[99] which has been shown to be a necessary ingredient for rate simulations.[100,101] Just as above, we recommend that this velocity reversal be invoked only if a frustrated hop is initiated by the derivative coupling.

3. RESULTS

To test the validity of our method, we will make the standard, simple approximation of a pair of parabolic diabatic PESs

$$U_0(x) = \frac{1}{2}m\omega^2x^2 \tag{32a}$$

$$U_1(x) = U_0(x) + \epsilon_d(x) = \frac{1}{2}m\omega^2(x-x_1)^2 + \Delta \tag{32b}$$

We will discuss more realistic Hamiltonians in Section 4. For the present, parabolic Anderson–Holstein model, a great deal is known about the relevant nonadiabatic dynamics. In the $kT \gg \hbar\omega \gg \Gamma$ limit, the electron transfer rate can be calculated by the Fermi's Golden rule and reduces to the Marcus theory of electrochemical electron transfer

https://dx.doi.org/10.1021/acs.jctc.0c00997
J. Chem. Theory Comput. 2021, 17, 614−626

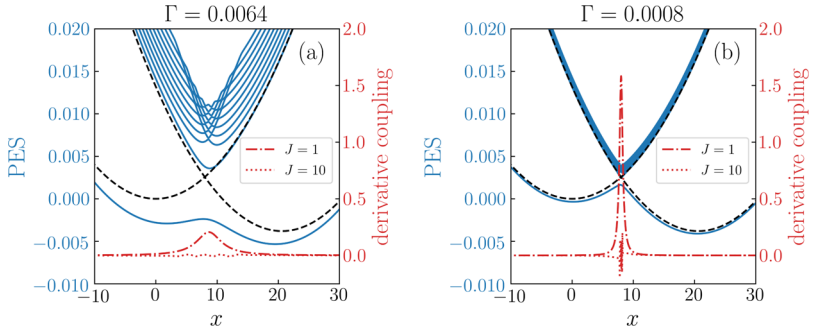

Figure 4. Subspace adiabatic PESs and derivative couplings with (a) $\Gamma = 0.0064$, and (b) $\Gamma = 0.0008$. In both figures, the one-electron metal states $\{\epsilon_k\}$ are evenly spaced and range from -0.2 to 0.2 with a spacing of $\Gamma/6.4$. The other parameters are $m = 2000$, $\omega = 0.0002$, $x_0 = 0$, $x_1 = 20.6097$, and $\Delta = -0.0038$. The ground adiabatic PES and ten lowest excited PESs are plotted in solid lines. The diabatic PESs (eqs 32a and 32b) are plotted in dashed lines for reference. The derivative coupling between the ground state and the first excited state peaks at the diabatic crossing. For higher excited states, the derivative couplings with the ground state are much smaller. Note that there is a finite gap between the ground and excited PES, indicating that pure-bath excitations of the ground state are excluded.

$$k_{\text{Marcus}} = k_{0\to 1} + k_{1\to 0} \tag{33a}$$

$$k_{0\to 1} = \int_{-\infty}^{+\infty} \mathrm{d}\epsilon f(\epsilon)\frac{\Gamma(\epsilon)}{\hbar}\sqrt{\frac{1}{4\pi E_r kT}} \exp\left(-\frac{(E_r + \Delta - \epsilon)^2}{4E_r kT}\right) \tag{33b}$$

$$k_{1\to 0} = \int_{-\infty}^{+\infty} \mathrm{d}\epsilon (1 - f(\epsilon))\frac{\Gamma(\epsilon)}{\hbar}\sqrt{\frac{1}{4\pi E_r kT}} \exp\left(-\frac{(E_r - \Delta + \epsilon)^2}{4E_r kT}\right) \tag{33c}$$

Here, $E_r \equiv m\omega^2 x_1^2/2$ is the reorganization energy and $\Gamma(\epsilon) \equiv 2\pi\sum_k |V_k|^2\delta(\epsilon - \epsilon_k)$. In the $kT, \Gamma \gg \hbar\omega$ limit, the rate is given by TST

$$k_{\text{TST}} = \kappa\frac{\omega}{2\pi} \mathrm{e}^{-U^{(b)}/kT} \tag{34}$$

where $U^{(b)}$ is the barrier height and κ is the transmission coefficient.

For simplicity, the system is taken to be in the wide-band limit, and Γ is also assumed to be independent of $\boldsymbol{R}$ so that the discussion on characteristic energy scales becomes more straightforward. In other words, we assume that (i) the set of energies $\{\epsilon_k\}$ spans a sufficiently wide range and (ii) the hybridization function is a constant. The parameters used in our simulation are $m = 2000$, $\omega = 0.0002$, $x_1 = 20.6097$, $\Delta = -0.0038$. The metal states $\{\epsilon_k\}$ span from -0.2 to 0.2 and are evenly spaced. The number of metal states is chosen to converge the PESs and derivative couplings, as will be discussed below. The temperature in our simulation is chosen to be $kT = 9.5 \times 10^{-4}$.

3.1. PESs and Derivative Couplings. In Figure 4, we plot the adiabatic PESs and the derivative couplings between the ground state and the excited states, with (a) $\Gamma = 0.0064$ and (b) $\Gamma = 0.0008$. The energy spacing between metal orbitals $(\delta\epsilon_k)$ is 1×10^{-3} and 1.25×10^{-4}, respectively, which is about $\Gamma/6.4$. In both cases, the ground PESs have the shape of a double well, and the lowest excited PESs recover the diabatic PESs asymptotically. The derivative coupling between the ground state and the first excited state peaks around the diabatic crossing point and is nearly zero elsewhere. As Γ becomes smaller, all the PESs approach the diabatic PESs, and the derivative couplings grow but narrow at the diabatic crossing point. Thus, our calculations seem analogous to the electronic structure in solution with Γ playing the role of the diabatic coupling V. Note that this analogy cannot be strictly correct, given that V applies when there are two electronic states, and $\Gamma \sim 2\pi V^2\rho$ applies when there is a continuous density-of-states.

To better understand Figure 4, note that, for the full Hamiltonian in eq 1, one expects that the lowest possible excitation energy will be roughly the energy spacing between metal orbitals, $\delta\epsilon_k$. After all, low-lying metal excitations are always possible. Thus, as $\delta\epsilon_k$ approaches zero, so should the excitation gap. Here, however, we find that the excitation gap near the diabatic crossing converges to a finite value close to Γ, as shown in Figure 5. Apparently, by choosing a CIS subspace

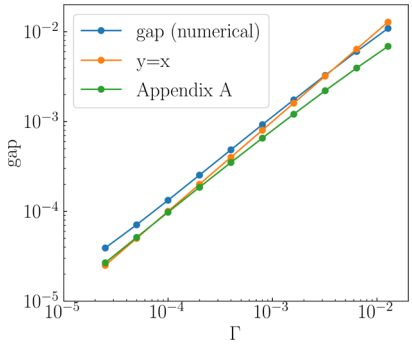

Figure 5. Excitation gap at the diabatic crossing vs hybridization Γ. A rough explanation for why the gap $\approx \Gamma$ is given in Appendix A.

to reflect charge-transfer excitations alone, we have successfully excluded pure-bath excitations above the ground state (with energies lower than the lowest charge-transfer excitation). In doing so, we have dramatically reduced the computational cost of the FSSH-ER approach, allowing one to focus on the adiabatic states with large derivative couplings to the ground state. Moreover, as shown in Figure 6, the derivative couplings between high-energy states with the ground state do become small. Thus, we expect that a simulation of charge-transfer dynamics in our reconstructed system can (at least sometimes) be performed with merely a handful of PESs. Finally, for a rough explanation of why the energy gap between the ground

https://dx.doi.org/10.1021/acs.jctc.0c00997
J. Chem. Theory Comput. 2021, 17, 614−626

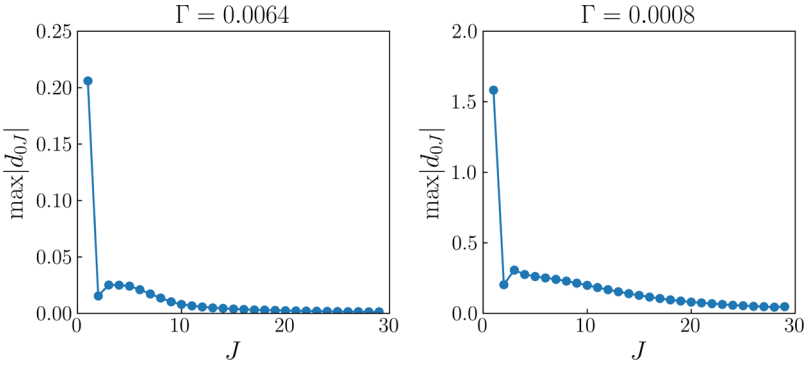

Figure 6. Maximum derivative couplings between the ground state and excited states. Note that the derivative couplings become small in all cases for higher excited states (and sometimes much faster).

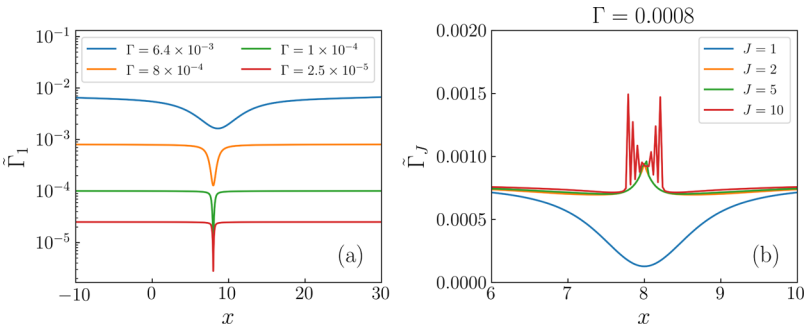

Figure 7. Relaxation $\tilde{\Gamma}$ (eq 15) as a function of the nuclear coordinate. The parameters are the same as those in Figure 4. The diabatic PESs cross at $x = 8.0011$. (a) $\tilde{\Gamma}$ for the first excited state at four different hybridization Γ's. Note that, except for the vicinity of the crossing, we find $\tilde{\Gamma}_1 \approx \Gamma$. For $\tilde{\Gamma}_1$, a ditch is always present near the crossing, highlighting the idea that nonadiabatic nuclear dynamics dominates at the crossing point (where the derivative coupling is large), but standard ER (whereby molecular electrons exchange with the metal) dominates everywhere else. (b) $\tilde{\Gamma}_J$ for $J = 1$, 2, 5, 10 at $\Gamma = 0.0008$. Unlike $\tilde{\Gamma}_1$, $\tilde{\Gamma}_J$ for higher-excited states can exhibit a bump ($J = 2$ and 5) or even an intriguing oscillating pattern ($J = 10$) near the crossing.

state and excited states seemingly approaches the value of Γ per se, please see Appendix A.

3.2. Relaxation $\tilde{\Gamma}(E_J)$. One major difference between our method and conventional FSSH or IESH is the presence of explicit ER as characterized by $\tilde{\Gamma}_J(E_J)$ and defined in eq 15. In Figure 7a, we plot $\tilde{\Gamma}_1$ (the relaxation for the first excited state) as a function of nuclear coordinates at four different hybridization Γ. We find that, when the nuclear coordinates are far away from the diabatic crossing, $\tilde{\Gamma}_1 \approx \Gamma$, which agrees with our intuition of ER (i.e., independent of nuclear motion). Interestingly, $\tilde{\Gamma}_1$ displays a dip at the diabatic crossing (where the derivative coupling is large), and the relative depth of this dip increases as Γ decreases. This state of affairs gives us a satisfying view of nonadiabatic effects at a molecule−metal interface: at the crossing point, there is a large derivative coupling (to accommodate nuclei switching surfaces) and a small $\tilde{\Gamma}$ (to accommodate ER, i.e., independent of nuclear motion); far from a crossing point, however, one finds a large $\tilde{\Gamma}$ and a small derivative coupling.

Next, we turn our attention to the behavior of $\tilde{\Gamma}_J$ as a function of excitation state energy. In Figure 7b, we plot $\tilde{\Gamma}_J$ for $J = 1$, 2, 5, 10 at $\Gamma = 0.0008$. For higher excited states, we continue to find that $\tilde{\Gamma}_J \approx \Gamma$ far from the crossing. However, in the vicinity of the crossing, $\tilde{\Gamma}_2$ and $\tilde{\Gamma}_5$ have a bump rather than a dip, and $\tilde{\Gamma}_{10}$ displays a curious oscillating pattern. Apparently, it is difficult to find an intuitive picture of nonadiabatic effects between many electronic states in the limit of a continuum: the Born−Oppenheimer formalism of generating adiabatic states is not directly compatible with a reduced description of charge transfer, and all of the complications created by the Born−Oppenheimer treatment lead to very intriguing behavior of the high-lyding excited state $\tilde{\Gamma}_J$ near the diabatic crossing. The form of these $\tilde{\Gamma}_J$ functions will be investigated in a future publication.

3.3. Electron Transfer Rate. Finally, in Figure 8, we compare the electron transfer rate predicted by FSSH-ER as a function of Γ with three other methods: (1) Marcus theory, which is valid in the small Γ limit; (2) TST, which is valid in

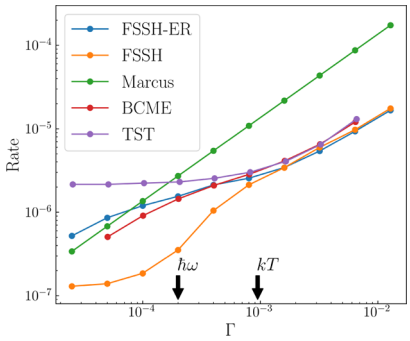

Figure 8. Rate of electron transfer as a function of Γ. The parameters are the same as those in Figure 4. Marcus theory is valid in the small Γ limit, and TST is valid in the large Γ limit ($\kappa = 0.5$). Overall both BCME and FSSH-ER are reliable across the full range of Γ. In the small Γ limit, FSSH-ER differs slightly from the Marcus rate in part because of a lack of decoherence.[102] For small Γ, ignoring the ER in the reduced system can significantly underestimate the rate.

https://dx.doi.org/10.1021/acs.jctc.0c00997
J. Chem. Theory Comput. 2021, 17, 614−626

the large Γ limit; and (3) BCME, which interpolates between both limits. These results have been previously reported in ref 90. To test the FSSH-ER method above, we perform a simulation with all trajectories initialized as the ground state of the left well and subject to an external nuclear friction $\gamma_n = 2m\omega$ (and the corresponding random force that obeys the fluctuation−dissipation theorem). Each data point is obtained by averaging over 2400 classical trajectories on 30 PESs. The rate is obtained by fitting $\langle d^\dagger d\rangle$ to the function $A\ e^{-kt} + B$, where k is the rate constant.

According to Figure 8, our method agrees with TST (with $\kappa = 0.5$) in the large Γ limit. In the small Γ limit, our method does predict a rate that decreases as Γ decreases, as does Marcus theory. However, for the smallest Γ, our method differs from the Marcus rate by about a factor of 1.6, and the slope is also different. Such differences are known for FSSH-like methods, especially without any decoherence,[102] which usually lead to an overestimate of the rate in the small Γ limit.

Finally, in Figure 8, we also plot data from a simulation which does not include any ER, that is, the electronic equation of motion obeys the quantum Liouville equation, and the surface switching algorithm merely considers the derivative couplings. In other words, we set $\mathcal{L} = 0$ in eqs 16a and 16b and $\zeta_{KJ} = 0$ in eq 29. As Figure 8 shows conclusively, for small Γ, ER in our simulation is crucial: the predicted rates are significantly underestimated without ER. Thus, Figure 8 would appear to validate a new picture of electron transfer at a metal surface that can interpolate between the TST limit (large Γ, with broadening) and the Marcus limit (small Γ); one can effectively include both derivative couplings and explicit ER at different points in the coordinate space.

4. DISCUSSION

Having demonstrated the power of the present FSSH-ER approach, let us now discuss several nuances of the approach as well as the future directions and possibilities.

4.1. Convergence Issues. For a realistic system, a metal contains a continuum of electronic states. For practical simulations, however, this continuum is always replaced by a set of discretized states that form a "quasi-continuum". One immediate question is, what is the criterion for a good quasi-continuum? Here, in our system-bath reconstruction procedure, we notice that the excitation gap and derivative couplings between our subspace adiabatic PESs seemingly converge when the energy spacing of this quasi-continuum is smaller than the hybridization Γ. This criterion poses a challenge for a system in the small Γ limit: for example, for a realistic calculation, this criterion would demand an ultra-dense Brillouin zone sampling. One possible solution would be to use Wannier interpolations.[103] For now, our intention is to use FSSH-ER only when a molecule is reasonably close to a surface so that Γ should not become too small. This circumstance is the most crucial case for electrochemical and catalytical simulations, as the limit $\Gamma \to 0$ can usually be treated perturbatively with Marcus theory (or some variant thereof).

Another question about convergence regards the number of PESs used in the dynamical simulation. For high-energy excited states, the derivative couplings (d_J) with the ground state becomes less significant, suggesting that there must be a natural cutoff. In this work, we used 30 PESs for our dynamical simulations based on the criterion $\max(|d_J|) < \max(|d_1|)/20$. However, such a cutoff based on relative magnitudes might not be sufficient; a cutoff based on the absolute magnitude might be necessary. Overall, assuming (1) there is no photoexcitation, (2) the system is initially thermally equilibrated, and (3) dynamics are initiated on the ground state, the present algorithm appears robust. Otherwise, the importance, relevance, and necessity of including many high-energy excited states will need to be addressed in the future.

4.2. Multiple Molecular Orbitals and Electron−Electron Interactions. In the present work, we consider only a noninteracting model where a molecule can be represented as a single impurity orbital. For realistic systems, such a model can hardly be adequate. Below, we will discuss two aspects that go beyond the model we considered above.

First, for many chemical problems of interest, there can be multiple molecular orbitals which are energetically relevant to a charge-transfer process near the metal surface. Suppose there are N energetically relevant molecular orbitals. One may project each orbital onto the occupied and virtual spaces individually, yielding N Schmidt occupied and virtual orbitals, respectively. Alternatively, if one uses a localized basis, one can perform a singular value decomposition to the molecular block of the occupied (virtual) orbitals and use the right-singular vectors to rotate the orbitals.[96,97] Thus, it is very likely that the present approach should be extendable to the case of many molecular orbitals, albeit with a higher computational cost. Indeed, in ref 93, we show how to generate relevant electronic states for a molecule composed of two molecular orbitals. However, in ref 93, we address only the ground state and not excited states or dynamics. Extending and benchmarking the present nonadiabatic formalism to the case of many molecular orbitals is a crucial step forward for this research.

Second, the inevitable elephant in the room, when we model electron transfer at a molecule−metal interface, is always the electron−electron interactions, which can scarcely be ignored in *ab initio* simulations. For a molecule alone, the Hartree−Fock approximation often gives qualitatively wrong results in the presence of strong e−e interactions, and one usually must resort to a higher level of electronic structure methods. Now obviously, for a molecule at a metal surface, Hartree−Fock is not an option, but DFT has proven to be very effective for modeling surface calculations. Because DFT takes the guise of an effective mean-field theory, the electronic structure and dynamics used above should be immediately applicable. In this regard, merging the current FSSH-ER formalism with DFT will be a top priority for future research.

Of course, if bonds are broken and/or one works in the small Gamma limit, standard DFT may fail and need to be adjusted. Now, in a previously published study, we have shown that, for an isolated and twisted C_2H_4 molecule, one can improve upon DFT by including one double excitation.[104] Moreover, in ref 93, we have also shown that including a subset of double excitations can vastly improve the performance of an electronic structure method describing a molecule on a metal surface (at least as far as ground state properties). In the future, it will be very exciting to merge FSSH-ER with *correlated* electronic structure techniques, for a truly robust view of nonadiabatic dynamics at a metal surface. This work is ongoing in our laboratory.

5. CONCLUSIONS

In this article, we have described a new method for simulating the coupled electronic-nuclear dynamics of a molecule near a metal surface with a special focus on molecular charge-transfer nonadiabatic effects. Starting with a molecule−metal system's

https://dx.doi.org/10.1021/acs.jctc.0c00997
J. Chem. Theory Comput. 2021, 17, 614−626

one-electron eigenstates, we build a set of configuration states where the impurity-related excitations can be distinguished from the pure-bath excitations. Next, a reduced representation is constructed for the purpose of dynamics. Then, based on this representation, we have proposed a modified surface hopping scheme with explicit ER. Finally, this method has been tested in a noninteracting Anderson−Holstein model, and we have extracted electron transfer rates. Our results appear valid across the full range of Γ.

Although the present work is limited to a noninteracting system with one impurity orbital, the framework established here can be easily extended to *ab initio* mean-field calculations with multiple impurity orbitals. We will also investigate multiple impurity orbitals with strong electron−electron interactions beyond mean field theory in the future. While practical questions do remain regarding how many states are required for convergence and the behavior of high-lying excited states in the reduced system, the FSSH-ER protocol appears to provide an efficient strategy for simulating molecular charge-transfer nonadiabatic dynamics both in the adiabatic and nonadiabatic regimes. Looking forward, our next step is to combine the present algorithm with *ab initio* electronic structure methods and hopefully make contact with realistic problems in electrochemistry and heterogeneous catalysis.

APPENDIX A

Estimate of the Excitation Gap at the Crossing

As mentioned in Section 3.1, by choosing a CIS subspace which excludes pure-bath excitations and focusing on charge-transfer excitations, we find a nonzero excitation gap in our redefined system. In this appendix, we will give a rough estimate of this gap near the diabatic crossing point.

Given any noninteracting impurity Hamiltonian

$$H = \begin{bmatrix} \epsilon_d & \cdots & V_k^* & \cdots \\ \vdots & \ddots & & \\ V_k & & \epsilon_k & \\ \vdots & & & \ddots \end{bmatrix} \tag{35}$$

the eigenvalues, denoted λ, are given by the characteristic equation $\det(\lambda I - H) = 0$, which is

$$(\lambda - \epsilon_d)\prod_k (\lambda - \epsilon_k) - \sum_k |V_k|^2 \prod_{k'}^{k'\neq k} (\lambda - \epsilon_{k'}) = 0 \tag{36}$$

Let us assume that bath states that do not couple to the impurity can be ignored, so that (1) $V_k \neq 0$ and (2) $\epsilon_k \neq \epsilon_{k'}$ for $k \neq k'$. (For the second assumption, if there are degenerate bath levels, we can always rotate them through a Householder reflection so that only one of them couples to the impurity). Therefore, eq 36 is equivalent to

$$\lambda - \epsilon_d - \sum_k \frac{|V_k|^2}{\lambda - \epsilon_k} = 0 \tag{37}$$

In other words, the eigenvalues of eq 35 are the roots of eq 37.

Now, the Hamiltonian for our reduced CIS subspace $\{|\Psi_{d_o}^{d_v}\rangle, |\Psi_{d_o}^{\tilde{a}}\rangle, |\Psi_{\tilde{i}}^{d_v}\rangle\}$ is of the form given in eq 35 and reads

$$\begin{aligned} H_{\mathrm{CIS}} &= (E_0 + \lambda_v - \lambda_o)I \\ &\quad + \begin{bmatrix} 0 & \langle d_v|H|\tilde{b}\rangle & \langle \tilde{j}|H|d_o\rangle \\ \langle \tilde{a}|H|\tilde{d}\rangle & \lambda_{\tilde{a}}\delta_{\tilde{a}\tilde{b}} - \lambda_v I & 0 \\ -\langle d_o|H|\tilde{i}\rangle & 0 & \lambda_o I - \lambda_{\tilde{i}}\delta_{\tilde{i}\tilde{j}} \end{bmatrix} \\ &\equiv (E_0 + \lambda_v - \lambda_o)I + \tilde{H}_{\mathrm{CIS}} \end{aligned} \tag{38}$$

here, $\lambda_{(\ldots)}$ represents the energy of a rotated orbital; for example, $\lambda_o \equiv \langle d_o|H|d_o\rangle$. The problem of finding the relevant excitation gap is equivalent to finding the smallest eigenvalue (λ) of $\tilde{H}_{\mathrm{CIS}}$ at the diabatic crossing, where $\langle d^\dagger d\rangle = 0.5$. We found numerically in Section 3.1 that $\lambda \approx \Gamma - \lambda_v + \lambda_o$ and we would like to confirm this result analytically.

To make progress, we begin by estimating the orbital energy of the Schmidt orbital $|d_o\rangle$ that is dual to the impurity. For simplicity, consider a band than spans from $-W$ to W with a constant hybridization function Γ. Assuming that the Fermi level $\epsilon_F = 0$, and the impurity on-site energy is $\epsilon_d = 0$. Then

$$\begin{aligned} \lambda_o &= \frac{1}{\langle n\rangle}\sum_i^{\mathrm{occ}} \lambda_i |\langle i|d\rangle|^2 \\ &= 2\int_{-W}^{0} \epsilon \frac{1}{\pi}\frac{\Gamma/2}{(\epsilon - \Lambda(\epsilon))^2 + (\Gamma/2)^2} d\epsilon \end{aligned} \tag{39}$$

where $\Lambda(\epsilon)$ is the real part of the self-energy. If we ignore $\Lambda(\epsilon)$ and assume that $W \gg \Gamma$, we can integrate eq 39 and λ_o can be approximated by

$$\lambda_o \approx -\frac{\Gamma}{\pi}\ln\left(\frac{2W}{\Gamma}\right) \tag{40}$$

Because we assume we are at the symmetric crossing point,

$$\lambda_v = -\lambda_o \tag{41}$$

Now, an eigenvalue of $\tilde{H}_{\mathrm{CIS}}$, denoted λ, must satisfy the self-consistent equation eq 37

$$\lambda = \sum_{\tilde{a}} \frac{|\langle \tilde{a}|H|d_v\rangle|^2}{\lambda - (\lambda_{\tilde{a}} - \lambda_v)} + \sum_{\tilde{i}} \frac{|\langle \tilde{i}|H|d_o\rangle|^2}{\lambda - (\lambda_o - \lambda_{\tilde{i}})} \tag{42}$$

As above, because we are at the symmetric crossing point, the two terms on the right hand side of eq 42 are equal. Finally, our task is to find the smallest λ which satisfies the equation

$$\lambda = 2\sum_{\tilde{a}} \frac{|\langle \tilde{a}|H|d_v\rangle|^2}{\lambda - (\lambda_{\tilde{a}} - \lambda_v)} \tag{43}$$

To solve eq 43, we begin by noticing that at the diabatic crossing

$$|d\rangle = \frac{1}{\sqrt{2}}(|d_o\rangle + |d_v\rangle) \tag{44}$$

Moreover, for any Hamiltonian of the form in eq 35, $|d\rangle$ can be expanded in the full set of eigenstates[105]

$$|d\rangle = \sum_p \frac{V}{\sqrt{\lambda_p^{\,2} + (\Gamma/2)^2}}|p\rangle \tag{45}$$

If we further assume the rotated bath orbitals can be approximated by the original bath orbitals, say $\tilde{a} \approx a$, then

https://dx.doi.org/10.1021/acs.jctc.0c00997
J. Chem. Theory Comput. 2021, 17, 614−626

$$\lambda \approx 4\sum_a \frac{V^2 {\lambda_a}^2}{{\lambda_a}^2 + (\Gamma/2)^2}\frac{1}{\lambda + \lambda_v - \lambda_a} = \frac{2\Gamma}{\pi}\int_0^W \frac{\epsilon^2}{\epsilon^2 + (\Gamma/2)^2}\frac{1}{\lambda + \lambda_v - \epsilon}d\epsilon = -\frac{2\Gamma}{\pi}\ln\left|\frac{r}{v}\right| - \frac{2\Gamma}{\pi}\frac{1}{v^2+1}(\mathrm{var}\ c\ \tan(r) + \ln|v|) \quad (46)$$

Here, in eq 46 we have defined

$$r \equiv \frac{2W}{\Gamma} \quad (47)$$

$$v \equiv 2(\lambda + \lambda_v)/\Gamma \quad (48)$$

Recall $\lambda_v \approx (\Gamma/\pi)\ln(2W/\Gamma) = (\Gamma/\pi)\ln(r)$ and denote

$$x \equiv \frac{\lambda + 2\lambda_v}{\Gamma} = \frac{\lambda}{\Gamma} + \frac{2}{\pi}\ln(r) \quad (49)$$

so that

$$v = 2\left(x - \frac{1}{\pi}\ln(r)\right) \quad (50)$$

In the end, eq 46 becomes (assuming $r \gg 1$ so that $\arctan(r) \approx \pi/2$)

$$x = \frac{2}{\pi}\frac{v^2}{v^2+1}\ln|v| - \frac{v}{v^2+1} \quad (51)$$

Equation 51 is a transcendental equation for x with parameter $r = 2W/\Gamma$. While there is no easy analytical solution, it is obvious that the solution is on the order of 1 for any reasonable r. In other words, from eq 49, $\lambda + 2\lambda_v = \lambda + \lambda_v - \lambda_o \approx \Gamma$.

AUTHOR INFORMATION

Corresponding Authors

Zuxin Jin − *Chemistry, University of Pennsylvania, Philadelphia, Pennsylvania 19104-6243, United States;* orcid.org/0000-0002-1533-3348; Email: zuxinjin@sas.upenn.edu

Joseph E. Subotnik − *Chemistry, University of Pennsylvania, Philadelphia, Pennsylvania 19104-6243, United States;* Email: subotnik@sas.upenn.edu

Complete contact information is available at: https://pubs.acs.org/10.1021/acs.jctc.0c00997

Notes

The authors declare no competing financial interest.

ACKNOWLEDGMENTS

This work was supported by the U.S. Air Force Office of Scientific Research (USAFOSR) AFOSR grants no. FA9550-18-1-0497 and FA9550-18-1-0420. Computational support was provided by the High Performance Computing Modernization Program (HPCMP) of the Department of Defense.

REFERENCES

(1) Wodtke, A. M.; Tully, J. C.; Auerbach, D. J. Electronically non-adiabatic interactions of molecules at metal surfaces: Can we trust the Born−Oppenheimer approximation for surface chemistry? *Int. Rev. Phys. Chem.* **2004**, *23*, 513−539.

(2) Bartels, C.; Cooper, R.; Auerbach, D. J.; Wodtke, A. M. Energy transfer at metal surfaces: the need to go beyond the electronic friction picture. *Chem. Sci.* **2011**, *2*, 1647−1655.

(3) Kandratsenka, A.; Jiang, H.; Dorenkamp, Y.; Janke, S. M.; Kammler, M.; Wodtke, A. M.; Bünermann, O. Unified description of H-atom−induced chemicurrents and inelastic scattering. *Proc. Natl. Acad. Sci. U.S.A.* **2018**, *115*, 680−684.

(4) Alemani, M.; Peters, M. V.; Hecht, S.; Rieder, K.-H.; Moresco, F.; Grill, L. Electric Field-Induced Isomerization of Azobenzene by STM. *J. Am. Chem. Soc.* **2006**, *128*, 14446−14447.

(5) Danilov, A. V.; Kubatkin, S. E.; Kafanov, S. G.; Flensberg, K.; Bjørnholm, T. Electron Transfer Dynamics of Bistable Single-Molecule Junctions. *Nano Lett.* **2006**, *6*, 2184−2190.

(6) Donarini, A.; Grifoni, M.; Richter, K. Dynamical Symmetry Breaking in Transport through Molecules. *Phys. Rev. Lett.* **2006**, *97*, 166801.

(7) Henningsen, N.; Franke, K. J.; Torrente, I. F.; Schulze, G.; Priewisch, B.; Rück-Braun, K.; Dokić, J.; Klamroth, T.; Saalfrank, P.; Pascual, J. I. Inducing the Rotation of a Single Phenyl Ring with Tunneling Electrons. *J. Phys. Chem. C* **2007**, *111*, 14843−14848.

(8) Jiang, B.; Alducin, M.; Guo, H. Electron−Hole Pair Effects in Polyatomic Dissociative Chemisorption: Water on Ni(111). *J. Phys. Chem. Lett.* **2016**, *7*, 327−331.

(9) Maurer, R. J.; Jiang, B.; Guo, H.; Tully, J. C. Mode Specific Electronic Friction in Dissociative Chemisorption on Metal Surfaces: H_2 on Ag(111). *Phys. Rev. Lett.* **2017**, *118*, 256001.

(10) Yin, R.; Zhang, Y.; Libisch, F.; Carter, E. A.; Guo, H.; Jiang, B. Dissociative Chemisorption of O2 on Al(111): Dynamics on a Correlated Wave-Function-Based Potential Energy Surface. *J. Phys. Chem. Lett.* **2018**, *9*, 3271−3277.

(11) Chen, J.; Zhou, X.; Zhang, Y.; Jiang, B. Vibrational control of selective bond cleavage in dissociative chemisorption of methanol on Cu(111). *Nat. Commun.* **2018**, *9*, 4039.

(12) Nienhaus, H.; Bergh, H. S.; Gergen, B.; Majumdar, A.; Weinberg, W. H.; McFarland, E. W. Electron-Hole Pair Creation at Ag and Cu Surfaces by Adsorption of Atomic Hydrogen and Deuterium. *Phys. Rev. Lett.* **1999**, *82*, 446−449.

(13) Gergen, B.; Nienhaus, H.; Weinberg, W. H.; McFarland, E. W. Chemically Induced Electronic Excitations at Metal Surfaces. *Science* **2001**, *294*, 2521−2523.

(14) Huang, Y.; Rettner, C. T.; Auerbach, D. J.; Wodtke, A. M. Vibrational Promotion of Electron Transfer. *Science* **2000**, *290*, 111−114.

(15) Krüger, B. C.; Meyer, S.; Kandratsenka, A.; Wodtke, A. M.; Schäfer, T. Vibrational Inelasticity of Highly Vibrationally Excited NO on Ag(111). *J. Phys. Chem. Lett.* **2016**, *7*, 441−446.

(16) Wagner, R. J. V.; Henning, N.; Krüger, B. C.; Park, G. B.; Altschäffel, J.; Kandratsenka, A.; Wodtke, A. M.; Schäfer, T. Vibrational Relaxation of Highly Vibrationally Excited CO Scattered from Au(111): Evidence for CO− Formation. *J. Phys. Chem. Lett.* **2017**, *8*, 4887−4892.

(17) Kumar, S.; Jiang, H.; Schwarzer, M.; Kandratsenka, A.; Schwarzer, D.; Wodtke, A. M. Vibrational Relaxation Lifetime of a Physisorbed Molecule at a Metal Surface. *Phys. Rev. Lett.* **2019**, *123*, 156101.

(18) Bünermann, O.; Jiang, H.; Dorenkamp, Y.; Kandratsenka, A.; Janke, S. M.; Auerbach, D. J.; Wodtke, A. M. Electron-hole pair excitation determines the mechanism of hydrogen atom adsorption. *Science* **2015**, *350*, 1346−1349.

(19) Dorenkamp, Y.; Volkmann, C.; Roddatis, V.; Schneider, S.; Wodtke, A. M.; Bünermann, O. Inelastic H Atom Scattering from Ultrathin Aluminum Oxide Films Grown by Atomic Layer Deposition on Pt(111). *J. Phys. Chem. C* **2018**, *122*, 10096−10102.

(20) Steinsiek, C.; Shirhatti, P. R.; Geweke, J.; Lau, J. A.; Altschäffel, J.; Kandratsenka, A.; Bartels, C.; Wodtke, A. M. Translational Inelasticity of NO and CO in Scattering from Ultrathin Metallic Films of Ag/Au(111). *J. Phys. Chem. C* **2018**, *122*, 18942−18948.

(21) Persson, B. N. J.; Persson, M. Vibrational lifetime for CO adsorbed on Cu(100). *Solid State Commun.* **1980**, *36*, 175−179.

(22) Andersson, S.; Persson, M. Inelastic electron scattering from surface vibrational modes of adsorbate-covered Cu(100). *Phys. Rev. B: Condens. Matter Mater. Phys.* **1981**, *24*, 3659−3662.
(23) Persson, M.; Hellsing, B. Electronic Damping of Adsorbate Vibrations on Metal Surfaces. *Phys. Rev. Lett.* **1982**, *49*, 662−665.
(24) Shenvi, N.; Roy, S.; Tully, J. C. Nonadiabatic dynamics at metal surfaces: Independent-electron surface hopping. *J. Chem. Phys.* **2009**, *130*, 174107.
(25) Roy, S.; Shenvi, N. A.; Tully, J. C. Model Hamiltonian for the interaction of NO with the Au(111) surface. *J. Chem. Phys.* **2009**, *130*, 174716.
(26) Shenvi, N.; Roy, S.; Tully, J. C. Dynamical Steering and Electronic Excitation in NO Scattering from a Gold Surface. *Science* **2009**, *326*, 829−832.
(27) Dou, W.; Subotnik, J. E. A broadened classical master equation approach for nonadiabatic dynamics at metal surfaces: Beyond the weak molecule-metal coupling limit. *J. Chem. Phys.* **2016**, *144*, 024116.
(28) Miao, G.; Dou, W.; Subotnik, J. Vibrational relaxation at a metal surface: Electronic friction versus classical master equations. *J. Chem. Phys.* **2017**, *147*, 224105.
(29) Rittmeyer, S. P.; Meyer, J.; Reuter, K. Nonadiabatic Vibrational Damping of Molecular Adsorbates: Insights into Electronic Friction and the Role of Electronic Coherence. *Phys. Rev. Lett.* **2017**, *119*, 176808.
(30) Spiering, P.; Meyer, J. Testing Electronic Friction Models: Vibrational De-excitation in Scattering of H2 and D2 from Cu(111). *J. Phys. Chem. Lett.* **2018**, *9*, 1803−1808.
(31) Elste, F.; Weick, G.; Timm, C.; von Oppen, F. Current-induced conformational switching in single-molecule junctions. *Appl. Phys. A* **2008**, *93*, 345−354.
(32) Bode, N.; Kusminskiy, S. V.; Egger, R.; von Oppen, F. Scattering Theory of Current-Induced Forces in Mesoscopic Systems. *Phys. Rev. Lett.* **2011**, *107*, 036804.
(33) Bode, N.; Kusminskiy, S. V.; Egger, R.; von Oppen, F. Current-induced forces in mesoscopic systems: A scattering-matrix approach. *Beilstein J. Nanotechnol.* **2012**, *3*, 144−162.
(34) Dzhioev, A. A.; Kosov, D. S.; von Oppen, F. Out-of-equilibrium catalysis of chemical reactions by electronic tunnel currents. *J. Chem. Phys.* **2013**, *138*, 134103.
(35) Galperin, M.; Ratner, M. A.; Nitzan, A. Molecular transport junctions: vibrational effects. *J. Phys.: Condens. Matter* **2007**, *19*, 103201.
(36) Galperin, M.; Nitzan, A. Nuclear Dynamics at Molecule−Metal Interfaces: A Pseudoparticle Perspective. *J. Phys. Chem. Lett.* **2015**, *6*, 4898−4903.
(37) Chen, F.; Miwa, K.; Galperin, M. Current-Induced Forces for Nonadiabatic Molecular Dynamics. *J. Phys. Chem. A* **2019**, *123*, 693−701.
(38) Chen, F.; Miwa, K.; Galperin, M. Electronic friction in interacting systems. *J. Chem. Phys.* **2019**, *150*, 174101.
(39) Scholz, R.; FloSS, G.; Saalfrank, P.; Füchsel, G.; Lončarić, I.; Juaristi, J. I. Femtosecond-laser induced dynamics of CO on Ru(0001): Deep insights from a hot-electron friction model including surface motion. *Phys. Rev. B: Condens. Matter Mater. Phys.* **2016**, *94*, 165447.
(40) Juaristi, J. I.; Alducin, M.; Saalfrank, P. Femtosecond laser induced desorption of ${\mathrm{H}}_{2},{\mathrm{D}}_{2}$, and HD from Ru(0001): Dynamical promotion and suppression studied with ab initio molecular dynamics with electronic friction. *Phys. Rev. B* **2017**, *95*, 125439.
(41) Lončarić, I.; Füchsel, G.; Juaristi, J.; Saalfrank, P. Strong Anisotropic Interaction Controls Unusual Sticking and Scattering of CO at Ru(0001). *Phys. Rev. Lett.* **2017**, *119*, 146101.
(42) Bouakline, F.; Fischer, E. W.; Saalfrank, P. A quantum-mechanical tier model for phonon-driven vibrational relaxation dynamics of adsorbates at surfaces. *J. Chem. Phys.* **2019**, *150*, 244105.
(43) Scholz, R.; Lindner, S.; Lončarić, I.; Tremblay, J. C.; Juaristi, J. I.; Alducin, M.; Saalfrank, P. Vibrational response and motion of carbon monoxide on Cu(100) driven by femtosecond laser pulses: Molecular dynamics with electronic friction. *Phys. Rev. B* **2019**, *100*, 245431.
(44) Fischer, E. W.; Werther, M.; Bouakline, F.; Saalfrank, P. A hierarchical effective mode approach to phonon-driven multilevel vibrational relaxation dynamics at surfaces. *J. Chem. Phys.* **2020**, *153*, 064704.
(45) Noga, J.; Bartlett, R. J. The full CCSDT model for molecular electronic structure. *J. Chem. Phys.* **1987**, *86*, 7041−7050.
(46) Bartlett, R. J.; Musiał, M. Coupled-cluster theory in quantum chemistry. *Rev. Mod. Phys.* **2007**, *79*, 291−352.
(47) Sherrill, C. D. *Annual Reports in Computational Chemistry*; Elsevier, 2005; Vol. *1*, pp 45−56.
(48) Meyer, H.; Miller, W. H. A classical analog for electronic degrees of freedom in nonadiabatic collision processes. *J. Chem. Phys.* **1979**, *70*, 3214−3223.
(49) Stock, G.; Thoss, M. Semiclassical Description of Nonadiabatic Quantum Dynamics. *Phys. Rev. Lett.* **1997**, *78*, 578−581.
(50) Meyer, H.-D.; Manthe, U.; Cederbaum, L. S. The multi-configurational time-dependent Hartree approach. *Chem. Phys. Lett.* **1990**, *165*, 73−78.
(51) Manthe, U.; Meyer, H. D.; Cederbaum, L. S. Wave-packet dynamics within the multiconfiguration Hartree framework: General aspects and application to NOCl. *J. Chem. Phys.* **1992**, *97*, 3199−3213.
(52) Beck, M.; Jäckle, A.; Worth, G.; Meyer, H.-D. The multiconfiguration time-dependent Hartree (MCTDH) method: a highly efficient algorithm for propagating wavepackets. *Phys. Rep.* **2000**, *324*, 1−105.
(53) Wang, H.; Thoss, M. Multilayer Formulation of the Multiconfiguration Time-Dependent Hartree Theory. *J. Chem. Phys.* **2003**, *119*, 1289−1299.
(54) Wang, H.; Thoss, M. Numerically Exact Quantum Dynamics for Indistinguishable Particles: The Multilayer Multiconfiguration Time-Dependent Hartree Theory in Second Quantization Representation. *J. Chem. Phys.* **2009**, *131*, 024114.
(55) Ben-Nun, M.; Martínez, T. J. Nonadiabatic molecular dynamics: Validation of the multiple spawning method for a multidimensional problem. *J. Chem. Phys.* **1998**, *108*, 7244−7257.
(56) Tanimura, Y.; Kubo, R. Time Evolution of a Quantum System in Contact with a Nearly Gaussian-Markoffian Noise Bath. *J. Phys. Soc. Jpn.* **1989**, *58*, 101−114.
(57) Tanimura, Y. Nonperturbative Expansion Method for a Quantum System Coupled to a Harmonic-Oscillator Bath. *Phys. Rev. A: At., Mol., Opt. Phys.* **1990**, *41*, 6676−6687.
(58) Tanimura, Y. Stochastic Liouville, Langevin, Fokker−Planck, and Master Equation Approaches to Quantum Dissipative Systems. *J. Phys. Soc. Jpn.* **2006**, *75*, 082001.
(59) Ishizaki, A.; Tanimura, Y. Quantum Dynamics of System Strongly Coupled to Low-Temperature Colored Noise Bath: Reduced Hierarchy Equations Approach. *J. Phys. Soc. Jpn.* **2005**, *74*, 3131−3134.
(60) Ishizaki, A.; Fleming, G. R. Unified Treatment of Quantum Coherent and Incoherent Hopping Dynamics in Electronic Energy Transfer: Reduced Hierarchy Equation Approach. *J. Chem. Phys.* **2009**, *130*, 234111.
(61) Mühlbacher, L.; Rabani, E. Real-Time Path Integral Approach to Nonequilibrium Many-Body Quantum Systems. *Phys. Rev. Lett.* **2008**, *100*, 176403.
(62) Chen, H.-T.; Cohen, G.; Millis, A. J.; Reichman, D. R. Anderson-Holstein Model in Two Flavors of the Noncrossing Approximation. *Phys. Rev. B: Condens. Matter Mater. Phys.* **2016**, *93*, 174309.
(63) Chen, H.-T.; Cohen, G.; Reichman, D. R. Inchworm Monte Carlo for Exact Non-Adiabatic Dynamics. I. Theory and Algorithms. *J. Chem. Phys.* **2017**, *146*, 054105.
(64) Chen, H.-T.; Cohen, G.; Reichman, D. R. Inchworm Monte Carlo for Exact Non-Adiabatic Dynamics. II. Benchmarks and Comparison with Established Methods. *J. Chem. Phys.* **2017**, *146*, 054106.

https://dx.doi.org/10.1021/acs.jctc.0c00997
J. Chem. Theory Comput. 2021, 17, 614−626

(65) Huo, P.; Coker, D. F. Iterative Linearized Density Matrix Propagation for Modeling Coherent Excitation Energy Transfer in Photosynthetic Light Harvesting. *J. Chem. Phys.* **2010**, *133*, 184108.
(66) Huo, P.; Coker, D. F. Communication: Partial Linearized Density Matrix Dynamics for Dissipative, Non-Adiabatic Quantum Evolution. *J. Chem. Phys.* **2011**, *135*, 201101.
(67) Thoss, M.; Kondov, I.; Wang, H. Correlated electron-nuclear dynamics in ultrafast photoinduced electron-transfer reactions at dye-semiconductor interfaces. *Phys. Rev. B: Condens. Matter Mater. Phys.* **2007**, *76*, 153313.
(68) Schinabeck, C.; Erpenbeck, A.; Härtle, R.; Thoss, M. Hierarchical quantum master equation approach to electronic-vibrational coupling in nonequilibrium transport through nano-systems. *Phys. Rev. B: Condens. Matter Mater. Phys.* **2016**, *94*, No. 201407(R).
(69) Xu, M.; Liu, Y.; Song, K.; Shi, Q. A non-perturbative approach to simulate heterogeneous electron transfer dynamics: Effective mode treatment of the continuum electronic states. *J. Chem. Phys.* **2019**, *150*, 044109.
(70) Dou, W.; Nitzan, A.; Subotnik, J. E. Surface hopping with a manifold of electronic states. II. Application to the many-body Anderson-Holstein model. *J. Chem. Phys.* **2015**, *142*, 084110.
(71) Dou, W.; Nitzan, A.; Subotnik, J. E. Surface hopping with a manifold of electronic states. III. Transients, broadening, and the Marcus picture. *J. Chem. Phys.* **2015**, *142*, 234106.
(72) Smith, B. B.; Hynes, J. T. Electronic friction and electron transfer rates at metallic electrodes. *J. Chem. Phys.* **1993**, *99*, 6517−6530.
(73) Head-Gordon, M.; Tully, J. C. Molecular dynamics with electronic frictions. *J. Chem. Phys.* **1995**, *103*, 10137.
(74) Juaristi, J. I.; Alducin, M.; Muiño, R. D.; Busnengo, H. F.; Salin, A. Role of Electron-Hole Pair Excitations in the Dissociative Adsorption of Diatomic Molecules on Metal Surfaces. *Phys. Rev. Lett.* **2008**, *100*, 116102.
(75) Dou, W.; Nitzan, A.; Subotnik, J. E. Frictional effects near a metal surface. *J. Chem. Phys.* **2015**, *143*, 054103.
(76) Rittmeyer, S. P.; Meyer, J.; Juaristi, J. I. n.; Reuter, K. Electronic Friction-Based Vibrational Lifetimes of Molecular Adsorbates: Beyond the Independent-Atom Approximation. *Phys. Rev. Lett.* **2015**, *115*, 046102.
(77) Dou, W.; Subotnik, J. E. A many-body states picture of electronic friction: The case of multiple orbitals and multiple electronic states. *J. Chem. Phys.* **2016**, *145*, 054102.
(78) Askerka, M.; Maurer, R. J.; Batista, V. S.; Tully, J. C. Role of Tensorial Electronic Friction in Energy Transfer at Metal Surfaces. *Phys. Rev. Lett.* **2016**, *116*, 217601.
(79) Maurer, R. J.; Askerka, M.; Batista, V. S.; Tully, J. C. Ab initio tensorial electronic friction for molecules on metal surfaces: Nonadiabatic vibrational relaxation. *Phys. Rev. B: Condens. Matter Mater. Phys.* **2016**, *94*, 115432.
(80) Novko, D.; Blanco-Rey, M.; Alducin, M.; Juaristi, J. I. Surface electron density models for accurate ab initio molecular dynamics with electronic friction. *Phys. Rev. B: Condens. Matter Mater. Phys.* **2016**, *93*, 245435.
(81) Dou, W.; Miao, G.; Subotnik, J. E. Born-Oppenheimer Dynamics, Electronic Friction, and the Inclusion of Electron-Electron Interactions. *Phys. Rev. Lett.* **2017**, *119*, 046001.
(82) Dou, W.; Subotnik, J. E. Universality of electronic friction: Equivalence of von Oppen's nonequilibrium Green's function approach and the Head-Gordon−Tully model at equilibrium. *Phys. Rev. B* **2017**, *96*, 104305.
(83) Dou, W.; Subotnik, J. E. Perspective: How to understand electronic friction. *J. Chem. Phys.* **2018**, *148*, 230901.
(84) Dou, W.; Subotnik, J. E. Universality of electronic friction. II. Equivalence of the quantum-classical Liouville equation approach with von Oppen's nonequilibrium Green's function methods out of equilibrium. *Phys. Rev. B* **2018**, *97*, 064303.
(85) Roy, S.; Shenvi, N.; Tully, J. C. Dynamics of Open-Shell Species at Metal Surfaces. *J. Phys. Chem. C* **2009**, *113*, 16311−16320.
(86) Tully, J. C. Molecular dynamics with electronic transitions. *J. Chem. Phys.* **1990**, *93*, 1061.
(87) Dou, W.; Subotnik, J. E. Electronic friction near metal surfaces: A case where molecule-metal couplings depend on nuclear coordinates. *J. Chem. Phys.* **2017**, *146*, 092304.
(88) Miao, G.; Ouyang, W.; Subotnik, J. A comparison of surface hopping approaches for capturing metal-molecule electron transfer: A broadened classical master equation versus independent electron surface hopping. *J. Chem. Phys.* **2019**, *150*, 041711.
(89) Ouyang, W.; Dou, W.; Jain, A.; Subotnik, J. E. Dynamics of Barrier Crossings for the Generalized Anderson−Holstein Model: Beyond Electronic Friction and Conventional Surface Hopping. *J. Chem. Theory Comput.* **2016**, *12*, 4178−4183.
(90) Coffman, A. J.; Dou, W.; Hammes-Schiffer, S.; Subotnik, J. E. Modeling voltammetry curves for proton coupled electron transfer: The importance of nuclear quantum effects. *J. Chem. Phys.* **2020**, *152*, 234108.
(91) The cost relative to IESH will depend on the number of electronic states propagated.
(92) Chen, J.; Jin, Z.; Dou, W.; Subotnik, J. Electronic Structure for Multielectronic Molecules Near a Metal Surface. **2020**, arXiv:2009.11249 [physics].
(93) Foster, J. M.; Boys, S. F. Canonical configurational interaction procedure. *Rev. Mod. Phys.* **1960**, *32*, 300.
(94) Edmiston, C.; Ruedenberg, K. Localized atomic and molecular orbitals. *Rev. Mod. Phys.* **1963**, *35*, 457.
(95) Pipek, J.; Mezey, P. G. A fast intrinsic localization procedure applicable for abinitio and semiempirical linear combination of atomic orbital wave functions. *J. Chem. Phys.* **1989**, *90*, 4916−4926.
(96) Knizia, G.; Chan, G. K.-L. Density Matrix Embedding: A Simple Alternative to Dynamical Mean-Field Theory. *Phys. Rev. Lett.* **2012**, *109*, 186404.
(97) Wouters, S.; Jiménez-Hoyos, C. A.; Sun, Q.; Chan, G. K.-L. A Practical Guide to Density Matrix Embedding Theory in Quantum Chemistry. *J. Chem. Theory Comput.* **2016**, *12*, 2706−2719.
(98) Of course, as is well known, this argument is not exact and will get worse with time because of different forces on different surfaces, eventually requiring a decoherence correction. For now, however, this nuance can be safely ignored.
(99) Jasper, A. W.; Truhlar, D. G. Improved treatment of momentum at classically forbidden electronic transitions in trajectory surface hopping calculations. *Chem. Phys. Lett.* **2003**, *369*, 60−67.
(100) Jain, A.; Herman, M. F.; Ouyang, W.; Subotnik, J. E. Surface hopping, transition state theory and decoherence. I. Scattering theory and time-reversibility. *J. Chem. Phys.* **2015**, *143*, 134106.
(101) Jain, A.; Subotnik, J. E. Surface hopping, transition state theory, and decoherence. II. Thermal rate constants and detailed balance. *J. Chem. Phys.* **2015**, *143*, 134107.
(102) Subotnik, J. E.; Shenvi, N. A new approach to decoherence and momentum rescaling in the surface hopping algorithm. *J. Chem. Phys.* **2011**, *134*, 024105.
(103) Giustino, F.; Cohen, M. L.; Louie, S. G. Electron-phonon interaction using Wannier functions. *Phys. Rev. B: Condens. Matter Mater. Phys.* **2007**, *76*, 165108.
(104) Teh, H.-H.; Subotnik, J. E. The Simplest Possible Approach for Simulating S0−S1 Conical Intersections with DFT/TDDFT: Adding One Doubly Excited Configuration. *J. Phys. Chem. Lett.* **2019**, *10*, 3426−3432.
(105) Mahan, G. D. *Many-Particle Physics*; Springer Science & Business Media, 2013.

https://dx.doi.org/10.1021/acs.jctc.0c00997
J. Chem. Theory Comput. 2021, 17, 614−626